Hardware-in-the-Loop Test of an Open Loop Fuzzy Control Method for Decoupled Electro-Hydraulic Antilock Braking System

Andrei Aksjonov, *Member, IEEE,* Vincenzo Ricciardi, *Member, IEEE,* Klaus Augsburg, Valery Vodovozov, *Member, IEEE,* and Eduard Petlenkov

***Abstract*—To verify functionality of an intelligent open loop fuzzy-logic-based antilock braking system control method for four on-board motor drive electric sport utility vehicle a hardware-in-the-loop experiment is conducted in this paper. The experimental facility includes a novel decoupled electro-hydraulic brake test bed characterized by highly nonlinear dynamics and time-varying behavior. It reproduces real pressure dynamics of the brake circuit allowing for simulation of various tire-road adhesions conditions and brake blending scenarios. To cope with degradation of antilock braking system performance induced by unexpected changing environmental conditions, such as road surface, the developed fuzzy control features a very simple yet effective and robust road surface recognition tool with estimation of the peak braking demands. Thus, the fuzzy logic serves as a controller and road surface estimator simultaneously allowing for complex mathematical modelling and feedback control avoidance not sacrificing safety system's performance. The results indicate that the control method manages highly nonlinear and time-variant dynamics of the brake system and offers significant feasibility for optimal slip control at regenerative braking, ensuring fuzzy control's potentiality for real-time application.**

***Index Terms*—Fuzzy control, antilock braking system, electrohydraulic actuator, intelligent control, electric vehicles**

I. Introduction

In addition to transportation, vehicle technology must ensure safety of occupants, goods, and environment, which has higher priority than time or cost. For example, an excessive braking torque leads to wheels' lockage, what deteriorates vehicle steerability and significantly reduces braking force: the vehicle is able to neither turn and avoid collision nor decelerate as fast as practicable. To solve this problem, an active safety technology promoted from aerospace industry, antilock braking system (ABS), was applied to ground vehicles. The ABS aims at decelerating a vehicle as fast as possible along with simultaneous maintaining steerability during an emergency braking maneuver. Its superior goal is to enhance the braking, steering, and driving stability. Today, the ABS is a mandatory safety system in almost every country in the world [1].

The challenge of controlling an ABS for electric sport utility vehicle (e-SUV) is provoked by (i) system's high nonlinearity and significant time delay; (ii) controller's instant response capability and robustness to continuously varying system's states and environment; (iii) uncertainties and lack of knowledge about the plant; (iv) electric motor and electro-hydraulic brake (EHB) actuators efficient blending strategy for maximum energy recuperation. Despite continuous response, the robust control methods, such as sliding-mode (SMC) [2, 3], model predictive [4, 5], nonlinear proportional-integral-derivative (PID) [6], linear matrix inequality [7], fail to operate such complex systems as ABS for e-SUV due to fundamental lack of robustness to ill-defined variables and vagueness, and their inability to consider several system binding aspects simultaneously. Consequently, fuzzy set theory, which is capable of overcoming above mentioned problems, found its effective application in ABS control [8 – 10].

For instance, a Mamdani's fuzzy logic controller (FLC) was applied to electric vehicle [11], for an FLC combined with PID controller [12] and for a quasi-SMC accompanied with fuzzy-neural network estimator applied to a conventional passenger car [13]. In [14], the authors developed the ABS FLC that provides optimal slip for varying road conditions. Recently, another solution consisting of SMC and FLC cooperation was presented [15]. In [16], the fuzzy logic was used in road surface detection, and additional FLC – for pressure control that holds optimal wheels slip. The control method was first tested against a quarter-car hardware-in-the-loop (HIL) simulation. Later, road type recognition was enhanced with an artificial neural network and validated in simulation and real vehicle experiment [17]. Finally, a complex control method based on

A. Aksjonov is with Concept Development Department, ŠKODA AUTO a.s., Mladá Boleslav, 29301 Czech Republic (e-mail: andrei.aksjonov@skoda-auto.cz).

V. Ricciardi and K. Augsburg are with the Department of Automotive Engineering, Technische Universität Ilmenau, Ilmenau, 98693 Germany (e-mails: vincenzo.ricciardi@tu-ilmenau.de; klaus.augsburg@tu-ilmenau.de).

V. Vodovozov is with the Department of Electrical Power Engineering and Mechatronics, Tallinn University of Technology, Tallinn, 19086 Estonia (e-mail: valery.vodovozov@taltech.ee).

E. Petlenkov is with the Department of Computer Systems: Centre for Intelligent Systems, Tallinn University of Technology, Tallinn, 19086 Estonia (e-mail: eduard.petlenkov@taltech.ee).

fuzzy logic, which required three inputs and a state observer to detect road friction coefficient and to decide upon an optimal wheel slip, was developed and tested in simulation and on a real car [18]. An FLC in combination with SMC [19, 20] or H_∞ [21] led to significant improvement in electro-hydraulic servomechanism control via rapid adaptation to dynamic system's states variation and robustness to plant-environment correlation uncertainties. In [22], the scholars utilized ration of wheel equivalent linear acceleration to drive motor torque to detect and control vehicle skidding. Again fuzzy logic was applied in this instance to handle a balanced tradeoff between anti-skid control and vehicle acceleration performance.

Development and verification of safety systems on real vehicle is often expensive and time consuming. On the other hand, computer simulation does not always guarantee realistic environment for testing vehicle safety systems, such as ABS, traction control systems, electronic stability program, etc. Consequently, in recent years the researchers have extensively used HIL simulation tests that replicate vehicle subsystems, such as braking system, suspension, and steering rack while the rest of the vehicle is represented as a numerical model. The HIL testing provides real-time behavior of the studied vehicle system and enables significant cost and time reduction in development and testing stages [23, 24].

Despite complexity and inherent nonlinear characteristics, the electro-hydraulic systems due to their effectiveness, precision, and fast response are widely used in automotive industry (i.e. braking system, suspension, etc.) [25], where advance regulation strategies are necessary for high-performance of motion, force, or positioning control [26]. However, most of these systems are featured with additional challenges caused by flow-pressure relationship, like dead-zone due to valve spool overlap, oil leakage, oil temperature variation, etc. Hence, fuzzy set theory was successfully applied as a control method for multiple electro-hydraulic systems, what allowed for avoidance of difficult time- and environment-dependent mathematical model of a plant [27 – 29].

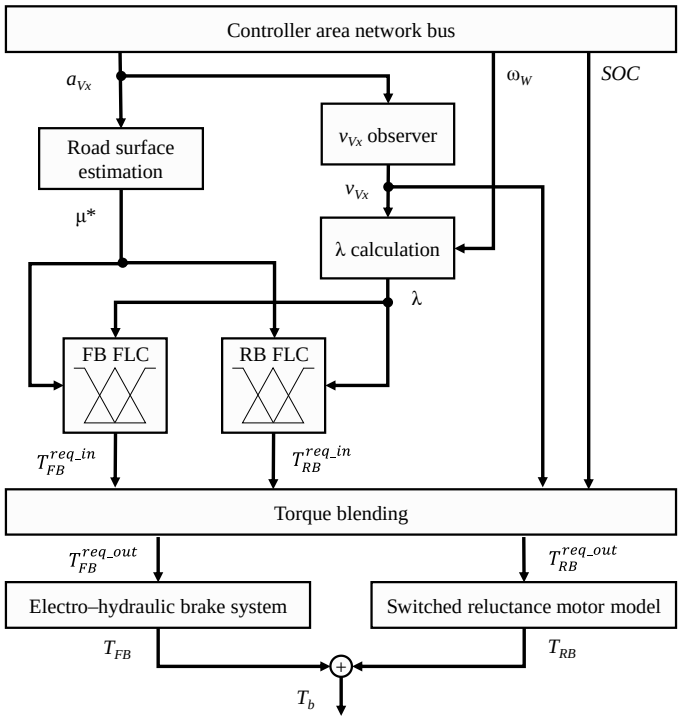

Fig. 1. Control method block scheme for a single wheel: RB FLC – regenerative brake fuzzy logic controller; FB FLC – friction brake fuzzy logic controller.

In previous study, the adaptability of the intelligent feedforward fuzzy control method for ABS for e-SUV with four independent in-wheel motors powertrain to dynamically changing and ill-defined environment conditions was investigated [30]. Although the simulation results proved control method's positive impact on ABS performance, it does not guarantee success on real system. Hence, testing the control method on HIL set up is an essential intermediate step before applying it to a real system. The main contribution of this paper is experimental verification and results demonstration of practical applicability of the previously proposed open loop FLC against HIL platform. The HIL setup consists of a novel decoupled EHB test bed developed by the ZF TRW Automotive (Koblenz, Germany) [31] and interconnected with a high fidelity vehicle dynamic software IPG CarMaker® (Karlsruhe, Germany), which runs experimentally validated e-SUV. The complexity of the HIL system under investigation is as follows:

- Separate control of each of the four wheels, whose performance influences each other and the overall system;
- Separate control of each of the four wheels via two fundamentally distinct actuators, i.e. decoupled EHB and electric motors;
- Collaboration between two actuators for ultimate goal of ABS performance and energy recuperation maximization;
- The delay of the EHB system induces significant loses in ABS performance.

The remaining of the paper is structured as follows. In the next Section, the open loop fuzzy-logic-based ABS control method for e-SUV is introduced. Section III is devoted to the decoupled EHB system and HIL setup description. The experimental results on low-μ and varying road conditions are presented in Section IV. The study is summarized in Section V.

II. Antilock Braking System Control Method

The main task of the ABS is fast vehicle deceleration by keeping vehicle handling stability and steerability. Additionally for the EVs, the ABS must guarantee maximum energy recuperation from the braking process. The feedforward FLC-based ABS control method (Fig. 1) recognizes road surface and holds optimal wheel slip deceleration on various road adhesions as well as in complex braking maneuvers for each wheel contemporaneously. It is managed by a single open loop FLC, which serves as a road surface identifier and a controller concurrently. Hence, complex mathematical modelling and set point-oriented control are avoided without sacrificing ABS's functionality. Efficient recuperation is provided by applying the maximum possible braking torque from the electric motors T_{RB}, and adding braking torque from a conventional EHB T_{FB} only when the torque generated by the electric motor is not sufficient to attain an optimal wheel slip λ_{opt} [30].

A. States Estimation

1) Road surface estimator μ*

A simplified schematic drawing of a braked wheel is depicted in Fig. 2. The tire-road adhesion coefficient μ is a ratio of the

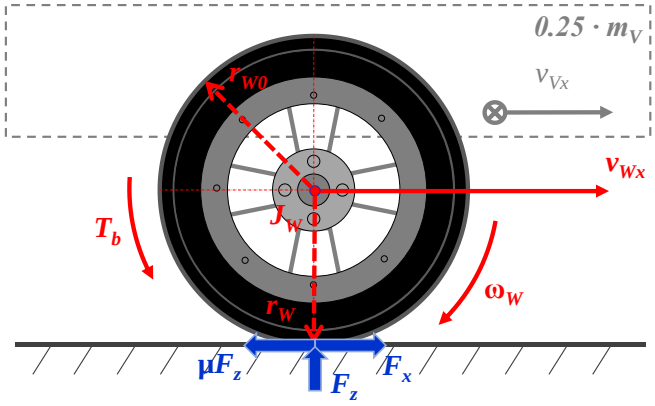

Fig. 2. A simplified drawing of a braked wheel.

applied longitudinal F_x and vertical F_z forces on a tire, and considering wheels' uniform adhesion, it is expressed as:

$$\mu = \frac{F_x}{F_z} = \frac{m_V \cdot a_{Vx}}{m_V \cdot g} = \frac{a_{Vx}}{g}, \quad (1)$$

where m_V and a_{Vx} are mass and longitudinal deceleration of a vehicle body respectively, and g is gravitational acceleration.

To estimate road surface under the tires μ*, the peak longitudinal deceleration value of the sensor is tracked. Moreover, during the braking process, μ* is reset with a certain frequency. While the variable is reset, the ABS is turned off allowing maximum requested braking torque on the wheels. In this period, a peak a_{Vx} is measured again. If the road surface remains unchanged, the same peak a_{Vx} is detected as in the previous step. However, if the road surface changes, the value of μ* is updated according to the road profile.

The method of road estimation proved to be very efficient in combination with fuzzy logic. In this case, it is necessary to know neither the peak deceleration rates nor the wheel optimal slips for every possible road surface. As to the limited available data about the wheel slip curves, computational intelligence methods based on fuzzy set theory, artificial neural networks, etc., can be used as an artificial decision making system to approximate the e-SUV's behavior for varying road surfaces from already known ones. In Table 1, the presented data are experimentally collected on different road surfaces and are true only for the studied vehicle and particular tire. These data are utilized in control method design. Conventional controllers, unlike soft computing methods, are not suitable for dealing with this type of stochastic and ill-defined information [32].

For instance, when the peak a_{Vx} is between wet and damp to any degree of certainty, it is not efficient to hold the λ_{opt} precisely for wet nor for damp road. The λ_{opt}, according to the tendency (Table I) lays somewhere between those two road surfaces. The fuzzy system processes this vague information using linguistic reasoning understandable for human. For example, fuzzy inference may be expressed in the *modus ponens* (**If** premise **Then** consequence) form as follows: **If** *road surface value is between wet and damp* **and** *wheel slip ratio is high for damp road*, **then** *decrease torque to obtain wheel slip ratio between optimal for wet and damp roads.*

TABLE I
OPTIMAL WHEELS' SLIP RATES AND VEHICLE'S BODY PEAK DECELERATION VALUES FOR COMMON ROAD SURFACES FOR STUDIED VEHICLE

	Icy	Wet	Damp	Dry
Font wheels λ_{opt} [%]	2.55	5.21	7.87	9.91
Rear wheels λ_{opt} [%]	2.76	6.11	8.89	11.57
Peak a_{Vx} [m/s^2]	2.69	5.09	7.62	10.10

2) Longitudinal wheel slip λ

In braking mode, the longitudinal wheel slip λ expressed in percentage is calculated as:

$$\lambda = \frac{v_{Vx} - v_{Wx}}{v_{Vx}} \cdot 100\%, \quad (2)$$

where longitudinal vehicle velocity v_{Vx} is an integration of a_{Vx}:

$$v_{Vx} = \int a_{Vx}\, dt, \quad (3)$$

and longitudinal wheel velocity v_{Wx} is derived from the measured wheel speed ω_W and radius of deformed tire r_W:

$$v_{Wx} = r_W \cdot \omega_W. \quad (4)$$

The radius of deformed tire is a relation of the stationary wheel ground contact force F_{z0} to the tire stiffness k_T in accordance with [33]:

$$r_W = r_{W0} - \frac{(F_z - F_{z_0})}{k_T}, \quad (5)$$

where r_{W0} is radius of undeformed tire and the wheel vertical load is approximated using a quasi-static longitudinal weight transfer approach [33]. In case of pure longitudinal driving without lateral acceleration, tire vertical forces for front (*f*) and rear (*r*) wheels are computed as:

$$\begin{cases} F_{z(f)} = m_V \left(\frac{l_r}{l} g - \frac{h_c}{l} a_{Vx} \right) \\ F_{z(r)} = m_V \left(\frac{l_f}{l} g + \frac{h_c}{l} a_{Vx} \right) \end{cases}, \quad (6)$$

where l_r and l_f are rear and front semi-wheelbase, l is wheel base, h_c is center-of-gravity height.

The friction (FB) and regenerative (RB) brake FLCs receive λ and μ* as inputs. The corresponding requested regenerative $T_{RB}^{req\_in}$ and friction $T_{FB}^{req\_in}$ braking torques are generated to keep an optimal slip for each wheel.

Remark 1: Pertinent sensors available in modern cars measure pressure of the EHB p_b and current of the on-board motor i, which are proportional to friction T_{FB} and regenerative braking torques T_{RB}, respectively. Hence, in this paper, the controller's corrective variables are RB torque for the motor and FB braking pressure for the EHB.

Remark 2: To reduce the noise in the sensors' signals, which is particularly important for the wheel longitudinal slip estimation (2), a linear Kalman filter [34] was applied.

B. Fuzzy Logic Controller

An FLC is composed of four main elements: fuzzification interface, inference engine, rule base, and defuzzification

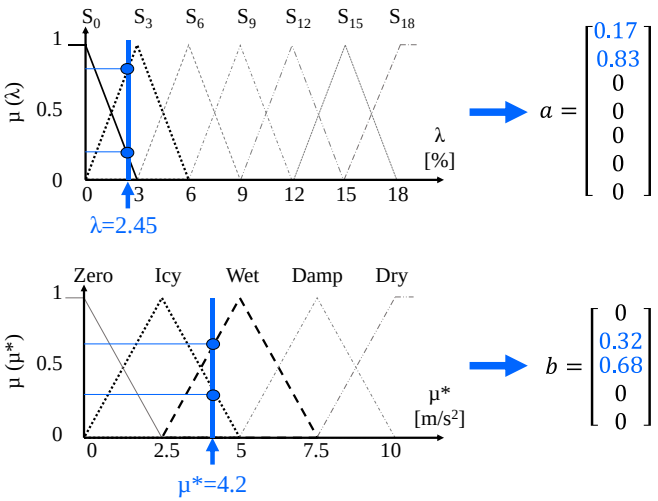

Fig. 3. FLC MFs and fuzzification procedure for randomly picked λ = 2.45 and μ* = 4.2: μ (λ / μ*) – degree of certainty of an FLC input.

interface. FLC takes a numerical value ("crisp") and transforms it into a linguistic variable in the fuzzification interface. Using a pre-defined rule base (a set of "*If-Then*" rules), the mapping between the input and output linguistic values is conducted by the inference engine. Finally, the defuzzification interface turns consequent linguistic output back into its crisp value [32].

1) Fuzzification

The first input of the FLC is the wheel slip λ. It has seven symmetrically dispersed and overlapping membership functions (MFs) over the whole universe of discourse (UOD) with a set of linguistic values {"*slip equals to 0*" (S_0); "*slip equals to 3*" (S_3); "*slip equals to 6*" (S_6); "*slip equals to 9*" (S_9); "*slip equals to 12*" (S_{12}); "*slip equals to 15*" (S_{15}); "*slip equals to 18*" (S_{18})}. Its UOD is bounded inside of [0 18] limit, which provides the range of values the λ can assume. The second crisp input is the estimated road surface μ*. It has five equal span and overlapping triangular MFs with linear fuzzy rule. The set of MF values is {"*Zero*"; "*Icy*"; "*Wet*"; "*Damp*"; "*Dry*"}. The UOD is restricted inside [0 10].

Symmetrical dispersion of the MFs over the UOD is responsible for equal MFs' sensitivity. Due to simplicity and fast response, all the inputs' MFs have triangular shape. The UOD limits are chosen based on the information about the plant, i.e. experimentally validated tire model (Table I).

In Fig. 3, the fuzzification process for the designed MFs for the FLC inputs is presented. The crisp inputs are fuzzified with a singleton (blue) function. As a result, two arrays *a* and *b* are obtained. Each position of the array corresponds to an appropriate MF linguistic value, and it contains a rate of its

TABLE II
FLC RULE BASE FOR REGENERATIVE BRAKING FOR FRONT / REAR WHEELS

$T_{RB}^{req\_in}$ [Nm]		μ* [m/s²]				
		Zero	*Icy*	*Wet*	*Damp*	*Dry*
λ [%]	S_0	60	80	160	200 / 120	200 / 140
	S_3	40	60	140	200 / 100	200 / 120
	S_6	20	40	120	200 / 60	200 / 100
	S_9	0	20	100	180 / 40	200 / 80
	S_{12}	0	0	60	160 / 20	200 / 40
	S_{15}	0	0	20	140 / 0	180 / 20
	S_{18}	0	0	0	120 / 0	160 / 0

TABLE III
FLC RULE BASE FOR FRICTION BRAKING FOR FRONT / REAR WHEELS

$p_b^{req\_in}$ [bar]		μ* [m/s²]				
		Zero	*Icy*	*Wet*	*Damp*	*Dry*
λ [%]	S_0	20	30	60	90 / 70	150 / 90
	S_3	10	20	50	80 / 50	130 / 80
	S_6	0	10	30	70 / 30	110 / 70
	S_9	0	0	10	50 / 10	90 / 50
	S_{12}	0	0	0	30 / 0	60 / 30
	S_{15}	0	0	0	10 / 0	30 / 10
	S_{18}	0	0	0	0 / 0	0 / 0

degree of membership (a value between 0 and 1) for a given input. When the input singleton does not intersect a MF, its array position value equals to zero. Thereafter, a dyadic product of two arrays is calculated resulting in matrix *C* [35]:

$$C = a \otimes b = ab^T. \tag{7}$$

2) Rule base and inference mechanism

A rule base captures the expert's knowledge about how to control the plant. Because a finite number of input MFs are designed, there is only a finite number of fuzzy rules. When there are not more than three inputs, a conventional way to list all possible sets of linguistic relations is to use a tabular representation [32].

The output of the RB FLC is the requested torque $T_{RB}^{req\_in}$. In total, it has eleven possible values starting from 0 to 200 with equal step of 20 between each variable. Its fuzzy rule base is presented in Table II for front and rear wheels. The requested FB pressure $p_b^{req\_in}$ is limited to 150 bar. Therefore, its consequent values from 0 to 150 form sixteen output options with a fixed step of 10 between each other. Input-output mapping of the FB FLC for front and rear wheels is introduced in Table III. Each FLC has 35 rules.

All the rule bases were obtained with a trial and error method, where the main criterion was to keep wheel slip as close as possible to its optimal rate. A linguistic quantification for one of the front wheels in regenerative braking may be expressed, for example, as follows: **If** wheel "*slip equals to 9*" **and** road surface is "*Wet*" **then** request from the electric motor regenerative braking torque equal to "*100*" Nm.

For inference engine, every rule base is converted into a matrix *R*. In Fig. 4, this transformation for RB front wheels FLC is shown. The same principle is applied to other rule bases. Finally, fuzzy inference is done via Hadamard product of two matrices of the same dimensions: *C* from the fuzzification interface, and *R* from the rule base [35]:

$$D = C \circ R. \tag{8}$$

$T_{RB(f)}^{req\_in}$ [Nm]		μ* [m/s²]				
		Zero	*Icy*	*Wet*	*Damp*	*Dry*
λ [%]	S_0	60	80	160	200	200
	S_3	40	60	140	200	200
	S_6	20	40	120	200	200
	S_9	0	20	100	180	200
	S_{12}	0	0	60	160	200
	S_{15}	0	0	20	140	180
	S_{18}	0	0	0	120	160

$$R = \begin{bmatrix} 60 & 80 & 160 & 200 & 200 \\ 40 & 60 & 140 & 200 & 200 \\ 20 & 40 & 120 & 200 & 200 \\ 0 & 20 & 100 & 180 & 200 \\ 0 & 0 & 60 & 160 & 200 \\ 0 & 0 & 20 & 140 & 180 \\ 0 & 0 & 0 & 120 & 160 \end{bmatrix}$$

Fig. 4. Front wheel RB FLC rule base (Table II) expression as matrix *R*.

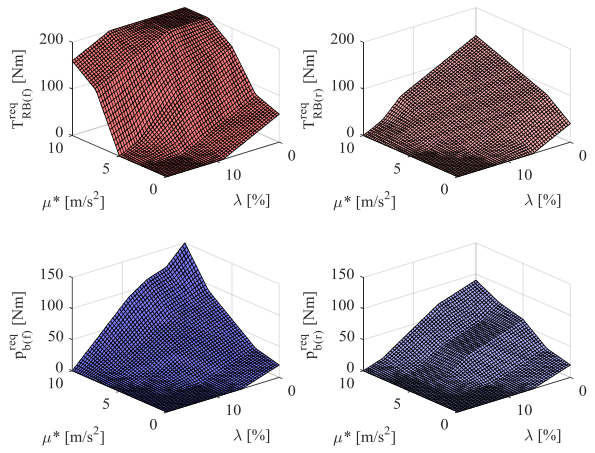

Fig. 5. FLC three-dimensional surfaces for regenerative braking and friction braking front (subscript '(*f*)') and rear wheels (subscript '(*r*)').

3) Defuzzification

The final element of every FLC is a defuzzification interface, where a resultative crisp output is obtained. Here the derived matrices *C* and *D* are converted into a single number. In this paper, a weighted average of the matrix elements is found. To this effect, a sum of elements in matrix *D* is divided by a sum of elements in matrix *C*. The calculation is shown for the RB requested torque on the front wheels [32]:

$$T_{RB(f)}^{req\_in} = \frac{\sum_{i=1;j=1}^{M:N} d_{ij}}{\sum_{i=1;j=1}^{M:N} c_{ij}}; \quad \begin{matrix} i=1,2,\ldots,N; \\ j=1,2,\ldots,M, \end{matrix} \tag{9}$$

where d_{ij} is an element of i^{th} row and j^{th} column of matrix *D* and c_{ij} is an element of i^{th} row and j^{th} column of matrix *C*.

In total, four different FLCs are designed for the e-SUV: two RB FLCs (i.e. for front and rear wheels), and two FB FLCs (i.e. for front and rear wheels). At last, the nonlinear three-dimensional surfaces for every FLC are generated (Fig. 5). Representation of the FLC controller with 2-input 1-output structure as a three-dimensional control surface is a common practice in fuzzy control theory [32]. The surfaces represent the outputs of the FLCs against their own inputs λ and μ* inside of the universe of discourse limits.

4) Stability analysis

The proposed open loop FLC does not involve a set-point reference inputs. Therefore, traditional stability analysis approaches, like Lyapunov's direct or indirect methods [32, 36], are not feasible. In this paper, the trajectory phase-plane analysis is used to refine the FLCs control surfaces (Fig. 5). It gives a visual assessment of the local stability and performance of studied nonlinear plant. It allows for analyzing the ability of the controller to prompt convergence to an equilibrium point taking into consideration the following stability condition [37]: *if the control is capable to stabilize the error and its derivative around the origin, then the control is locally stable*. The method is especially efficient for non-linear systems whereby analytical solutions for the proof of stability does not exist.

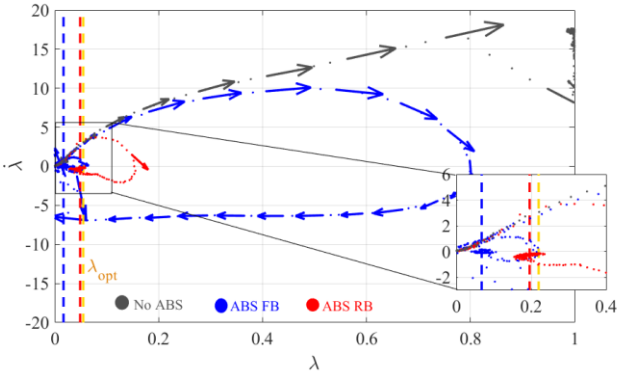

Fig. 6. Phase-plane diagram of slip ratio vs slip ratio derivative on low-μ road surface for front left wheel.

Time differentiation of (2) leads to the following statement:

$$\dot{\lambda} v_{Vx} + \lambda \dot{v}_{Vx} = \dot{v}_{Vx} - \dot{\omega}_W r_W. \tag{10}$$

Taking into account torque balance during the straight-line braking, the longitudinal wheel slip dynamics are expressed as:

$$\dot{\lambda} = \left(\frac{T_b - F_x(\lambda)\cdot r_W}{J_W}\right)\cdot\frac{r_W}{v_{Vx}} + \frac{\dot{v}_{Vx}}{v_{Vx}}\cdot(1-\lambda), \tag{11}$$

where J_W is moment of inertia of wheel.

The equilibrium point of (11) is characterized by $\dot{\lambda} = 0$, where the condition below is true:

$$\overline{T_b} = -\dot{v}_{Vx}\cdot(1-\bar{\lambda})\cdot\frac{J_W}{r_W} + F_x(\bar{\lambda})\cdot r_W, \tag{12}$$

In Fig. 6, the experimental results are represented on of the stability trajectory phase-plane analysis for front left wheel. The designed FLCs are activated. The arrows show the magnitude and direction of the wheel slip variation. The wheel slip is calculated applying (2), while the wheel slip rate is found in accordance to (11). In additional, the performance of the e-SUV without ABS activation is also shown.

With no ABS activated (gray), the wheels are locked, what leads to unstable behavior. Although the system reaches its stable equilibrium point, the FLC controlling the EHB (blue) takes significant time to reach the equilibrium. On the contrary, thanks to fast dynamics, the RB actuator (red) allows for a faster convergence of the system to the equilibrium. Despite the difference in convergence speed, both actuators operate inside of the safe wheel slip area, what has a higher priority in the framework of vehicle safety and steerability in emergency braking situation.

C. Torque Blending Strategy

The torque blending strategy is designed to prioritizing usage of electric motor for maximum energy recuperation for a given road surface. The EHB system is activated if the maximum motor torque for a certain speed is requested, and the tire slip value is lower than its optimal one for a given road. Furthermore, the strategy it also accounts for the battery's state of charge (*SOC*) switching between electric motors and EHB.

For this reason, the torque blending strategy is classified of series type, as the EHB is only activated when the request exceeds the motors performance. The outputs are the resultative RB and FB torques, $T_{RB}^{req\_out}$ and $T_{FB}^{req\_out}$, requested from the actuators. A schematic flowchart is shown in Fig. 7:

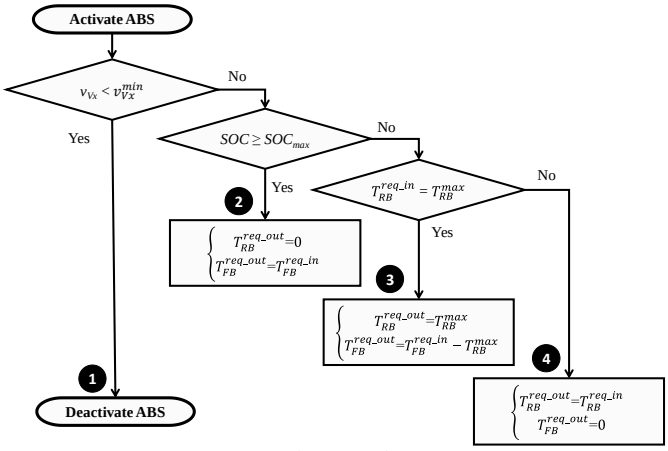

Fig. 7. Torque blending strategy flowchart for a single wheel

1. The algorithm checks the velocity of the vehicle: if the vehicle longitudinal speed v_{Vx} is smaller than the fixed minimum threshold v_{Vx}^{min} (e.g. 8 – 15 km/h), the ABS control is deactivated considering the difficulties of estimating the wheel slip [1];
2. When the *SOC* reaches the maximum allowed threshold SOC_{max} (e.g. 90%), the braking switches to pure FB mode;
3. The blended ABS considers the motor's peak performance: when peak torque T_{RB}^{max} of the SRM is requested by the FLC, the block supplies the peak torque request to the motor and calculates additional torque for the FB actuator to ensure optimal deceleration;
4. When none of the previous conditions are true, the EV decelerates only with motors as the ABS actuators.

At last, the braking torque T_b of the e-SUV is a sum of regenerative and friction torques (Fig. 1):

$$T_b = T_{RB} + T_{FB}. \tag{13}$$

III. Hardware-in-the-Loop Set-Up

A. Vehicle Configuration

An experimentally validated 14 degree-of-freedom vehicle model is provided by the IPG CarMaker® 6.0. The vehicle under investigation is an e-SUV equipped with decoupled EHB. Each wheel contains an electric drive connected through a half-shaft transmission that enables independent wheels control. The Pacejka's "Magic Formula" 6.1 is applied for tire modelling. The e-SUV configuration is introduced in Table IV.

TABLE IV
Vehicle Configuration

Parameters	Value	Unit
Mass	1963	kg
Wheelbase	2.665	m
Track width	1.625	m
Centre of gravity height	0.673	m
Drag coefficient	0.35	–
Frontal surface	2.323	m^2
Overall motor-gear ratio	1:10.56	–
Peak torque / power of a motor	200 / 100 (30 sec)	Nm / kW
Nominal torque / power of a motor	135 / 42	Nm / kW
Maximum speed of a motor	15000	min^{-1}

To reproduce real dynamics of the brake linings coefficient of friction, the Ostermeyer's model [33] is used. The model allows for an improved fidelity of the HIL platform, because it accounts for the brake linings' coefficient of friction dependence against speed, pressure, and temperature. It assumes that the friction coefficient is proportional to the total area of contact patches. The resulting patches area is determined by the equilibrium between the flow of growth (i.e. temperature related) and destruction (i.e. wear related). The model relies on two differential equations in the friction μ_b and temperature τ states:

$$\begin{cases} \dot{\mu}_b = -\alpha \cdot \{\mu_b \cdot (r_b \cdot \omega_W \cdot F_{cl} + \beta) - \gamma \cdot \tau\} \\ \dot{\tau} = \varepsilon \cdot r_b \cdot \omega_w \cdot F_{cl} - \delta \cdot (\tau - \tau_0) \end{cases}, \tag{14}$$

where r_b is effective braking radius, τ_0 is initial temperature of brake disc, and F_{cl} is a brake clamping force found as:

$$F_{cl} = A_p \cdot p_b, \tag{15}$$

where A_p is piston area of caliper.

Remark 3: the term $r_b \cdot \omega_W \cdot F_{cl}$ embeds the combined effect of clamping force and sliding speed, whilst the constant parameters α, β, γ, δ, and ε are attributable to the pad chemical formulation: (i) α is a time constant ruling the growth / destruction rate of the contact area and its current value; (ii) β is correlation parameter between the change rate of the contact area and its current value; (iii) γ correlates the change rate of the contact area to the temperature; (iv) ε rules the frictional power dissipated as heat on the contact patches; (v) δ refers to a brake cooling factor and rules the convection effect.

B. HIL Testbed

The decoupled EHB system shown in Fig. 8 is based on the slip control boost technology developed by the ZF TRW Automotive. The EHB system finds wide use in EV, because it ensures smooth coordination between FB and RB without the driver noticing it. Such a system also ensures faster response

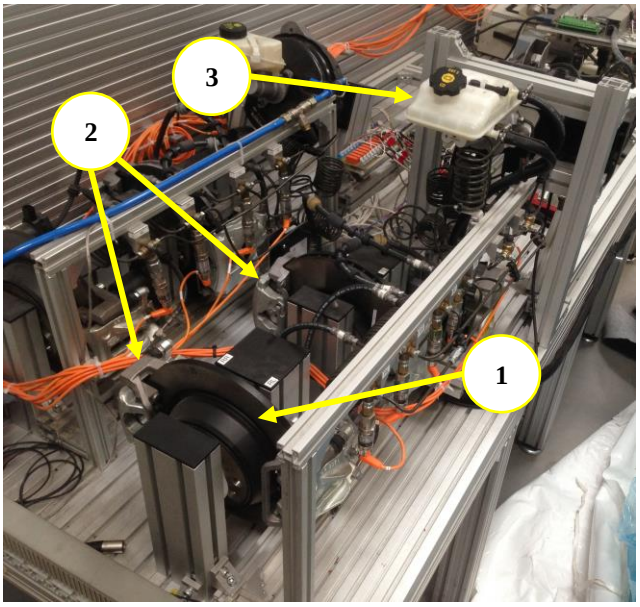

Fig. 8. The EHB HIL testbed: 1 – brake disk; 2 – brake caliper; 3 – master cylinder with reservoir.

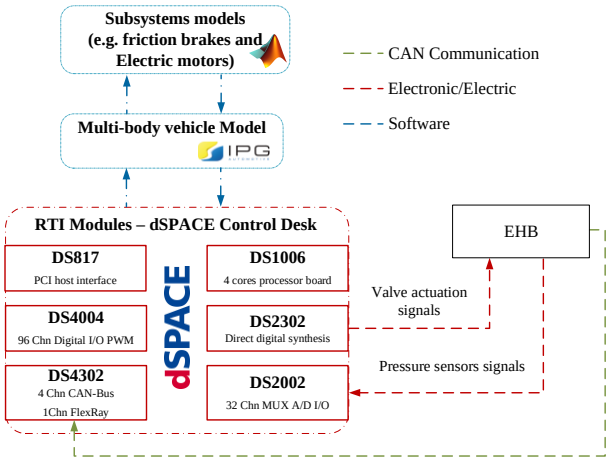

Fig. 9. Hardware and software communication: RTI – real-time interface; PCI – peripheral component interconnect; PWM – pulse width modulation; MUX – multiplexer.

time, more flexible packaging, and better integration with other chassis and powertrain control systems.

The hardware setup consists of the EHB and its control unit. The brake calipers are mounted on two discs, fixed with respect to the structure frame. The main task of the HIL is to reproduce real pressure dynamics of the brake circuit. The sensor measure the brake line pressure in the four brake calipers in a range from 0 to 20 MPa with cut-off frequency of 1 kHz.

The core HIL test rig is based on dSPACE® (Paderborn, Germany) modular platform with several hardware components responsible for data input / output, the control of the EHB and the communication with the vehicle simulator in IPG CarMaker® (Fig. 9). The latter runs the multibody e-SUV model parameterized according to experimental data. The dSPACE® unit converts signals from analogue to digital form and vice versa for real-time experiments.

The DS1006 board is the main element of the HIL platform. It is capable of distributing computing tasks between four core processors that guarantee real-time simulation. This board communicates via user datagram protocol with a local host personal computer (PC). Analog input signals information from the sensors of the brake system are digitalized by multi-channel A/D board DS2002. The DS2002 features a total of 32 A/D channels at 16-bit resolution with an ADC conversion time of less than 5 µs. The dSPACE® Control Desk software coordinates the test rig and allows for separate control of each actuator.

The EHB does not require the actuation of the brake pedal since the pressure request can be generated directly from software and sent via controller area network (CAN) bus to the EHB control module. For this task, one of the four CAN interfaces of the DS4302 is used. To configure the CAN network and to combine dSPACE® boards with CAN networks, the real-time interface multi-message blockset is used. The control on the EHB unit uses the direct digital synthesis board DS2302. This board can generate waveform signals and is required for the operation of emulators of wheel angular speed sensors. This latter is particularly important to account for the sensors' white noise.

The transfer function of the decoupled EHB system is experimentally assessed to be equal to:

$$\frac{T_{FB}}{T_{FB}^{req\_out\uparrow}} = \frac{1}{0.00075s^2+0.037s+1} e^{-0.026s}. \quad (16)$$

$$\frac{T_{FB}}{T_{FB}^{req\_out\downarrow}} = \frac{1}{0.00021s^2+0.045s+1} e^{-0.015s}. \quad (17)$$

Finally, the electric motor is represented as mathematical model. It is run in the multi-body vehicle model. Considering transmission gear ratio, the maximum torque applied directly to the wheel achieves 2100 Nm. The motor dynamics are described by the first-order transfer function [30]:

$$\frac{T_{RB}}{T_{RB}^{req\_out}} = \frac{1}{0.0022s+1} e^{-0.002s}. \quad (18)$$

IV. Hardware-in-the-Loop Experimental Results

To evaluate the developed control method on robustness to changing environmental conditions, the HIL experiment is conducted on multiple road surfaces and their transient combinations. In this paper, braking performance on low-µ and transient (i.e. from high-µ to low-µ) road surfaces are discussed in details. In all experiments, the vehicle is accelerated to 100 km/h, and then the maximum braking torque is requested.

A. *Low-µ Surface Experiment*

High-performance ABS is essential on low-µ surfaces (e.g. icy, wet), because on a slippery road the vehicle loses control very quickly. In this subsection, the results of heavy braking on a low-µ road surface (µ≈0.25) with blended braking control (Fig. 10) are presented, and are compared to the conventional FB (Fig. 11). The notations FL, FR, RL and RR refer to the front left, front right, real left and rear right wheels respectively.

1) Regenerative braking

In Fig. 10.a, the wheel speeds and vehicle longitudinal velocity diagrams for RB are plotted. The braking torques are generated by the electric motors only. Thus, the vehicle decelerates in full regenerative mode, as the FBs are not applied. Each wheel rotates almost with the same speed because the optimal wheel slip ratios are approximately the same for both the front and the rear wheels, roughly equal to 3 % (Table I). Thanks to its fast dynamics, the controller is able to maintain the optimal slip value for each wheel (Fig. 10.b).

In Fig. 10.b, the optimal wheel slip is also depicted as a black dashed line. Every two seconds peaks in the slip signals are observable. These are the results of the reset, which is used to understand whether the road surface is changed or not during the braking maneuver. Within this period, the road surface estimator applies the maximum braking torque (Fig. 10.c) and concurrently the road recognition is reset to null (Fig. 10.d).

In Fig. 10.c, the wheel RB torques are represented. The motors respond very fast allowing for precise and smooth control of the vehicle. Finally, in Fig. 10.d, the vehicle longitudinal deceleration a_{Vx} curve is shown along with a road recognition variable µ*, which represents the maximum braking potential. At the beginning of the heavy braking maneuver (i.e. at around 2 seconds), the controller detects maximum possible deceleration rate. Thereafter, the FLC

addresses this variable to an appropriate road surface (Table I), whose linguistic value is "*Icy*". As a result, thanks to optimal wheel slip control, a constant vehicle deceleration is maintained during the whole braking process. Therefore, high efficiency of a braking process is deemed with an enabled steerability.

2) Friction braking

In Fig. 11.a, the wheels' speeds and vehicle velocity are presented for the conventional FB case. In this experiment, the vehicle decelerates only by applying the FB torques supplied by the EHB. The difference between RB and FB results is easily noticeable. The wheel slip tracking of the FB (Fig. 11.b) has significant lower performance than the RB (Fig. 10.b). This phenomenon is attributable to the EHB (Eq. (16) – (17)) slower dynamics compared to the motor (Eq. (18)). Indeed, the FLC for the FB was tuned to optimize the optimal slip tracking performance (Table I) and avoid controller output oscillation detrimental to the EHB actuators. Therefore, the FLC FB efficiency is sensibly decreased.

In Fig. 11.c, the FB torques for each wheel are revealed. Comparing to RB (Fig. 10.c), the HIL system entails a slower but markedly oscillating dynamics that take a tool on the driving comfort. Nevertheless, both FLCs are requesting similar torque values for the front and rear wheels.

In Fig. 11.d, road detection together with vehicle body deceleration curve are presented. The vehicle deceleration rate is considerably lower than for the full RB scenario (Fig. 10.e).

TABLE V
RB AND FB ABS PERFORMANCE BENCHMARKING ON ICE ROAD SURFACE

Mode	Mean a_{Vx} [m/s^2]	$s_{braking}$ [m]	ABS_{IP}
RB	2.6009	151.8394	1.2535
FB	2.3589	170.9701	1.1368

The tracking of a slip value lower than its optimal value still ensures steerability but to the detriment of the braking force, which accordingly leads to efficiency losses.

3) Regenerative and friction braking performance comparison

Although the difference between the FLCs' performance for RB and FB is clearly visible in Fig. 10 and 11, the main ABS performance indexes are presented in Table V. The average deceleration rate for RB braking is higher comparing to the FB. Accordingly, the braking distance $s_{braking}$ of the RB is smaller than FB by almost 20 m, which is a significant result in vehicle safety. Furthermore, the ABS index of performance ABS_{IP} is considered to evaluate the system's efficiency. The variable is a ratio between the mean vehicle body decelerations achieved respectively with enabled controller and with locked wheels when no ABS control is applied:

$$ABS_{IP} = \frac{a_{Vx}^{ABS}}{a_{Vx}^{lock}}. \tag{19}$$

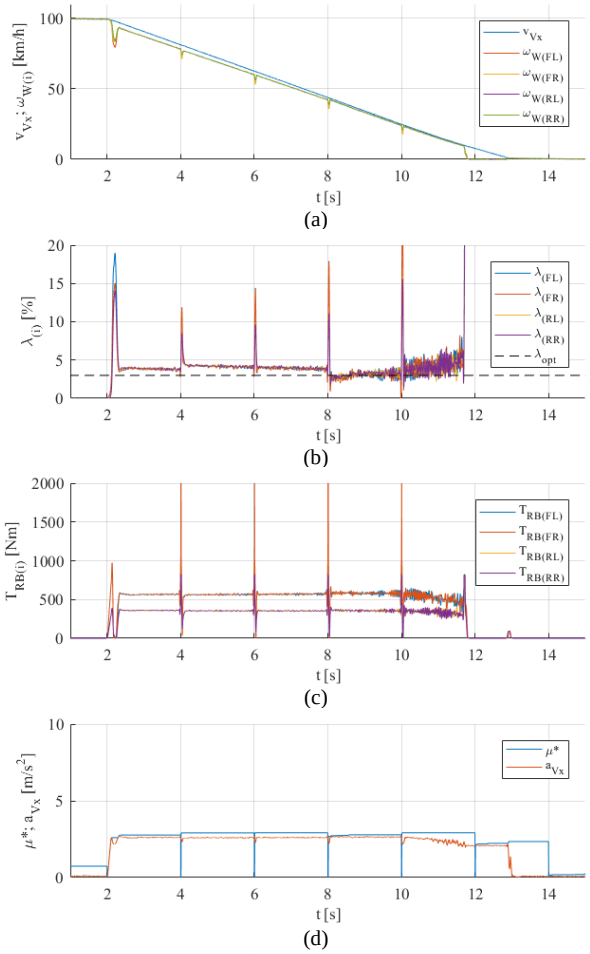

Fig. 10. Experimental results from braking on a low-μ (μ≈0.25) road surface for regenerative braking: (a) vehicle and wheels speeds (b) wheels longitudinal slips; (c) RB torques; (d) road detection with vehicle body deceleration.

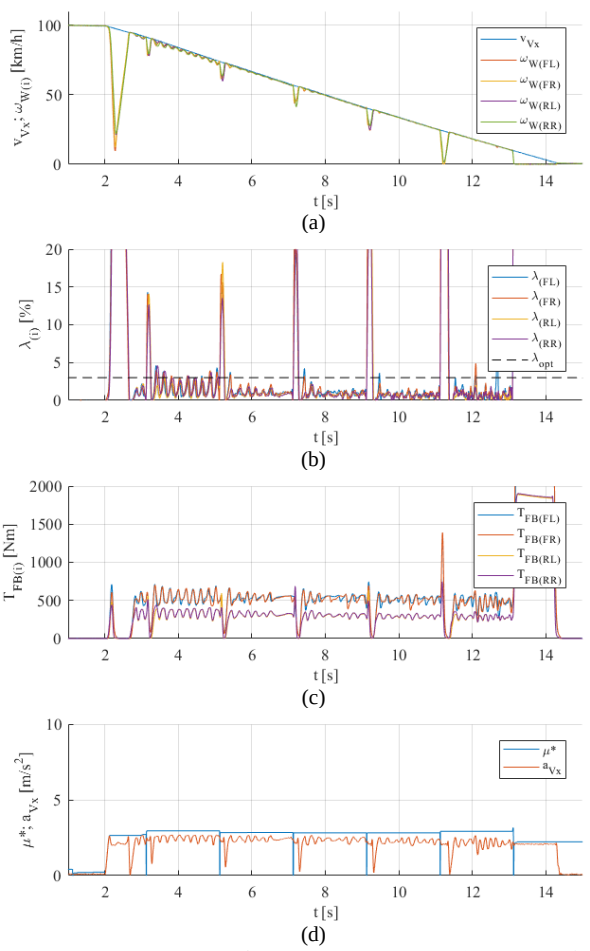

Fig. 11. Experimental results from braking on a low-μ (μ≈0.25) road surface for friction braking: (a) vehicle and wheels speeds (b) wheels longitudinal slips; (c) FB torques; (d) road detection with vehicle body deceleration.

B. Varying Road Conditions (From High-μ to Low-μ)

The road surfaces are rarely homogeneous. Hence, the results stemming from a heavy braking maneuver on changing road surface are reported. Particularly, the vehicle starts decelerating on a high-μ (μ≈1) surface and continues towards low-μ (μ≈0.25). For this test, the RB requires additional torque from the EHB, because the torque generated by on-board motor is not enough to reach optimal wheel slip.

1) Regenerative braking (blended)

In Fig. 12, the vehicle deceleration results in regenerative mode on a changing road surface are presented. The vehicle decelerates with higher wheel slip values at the beginning of the maneuver. Whilst the slip of the rear wheels is close to its optimal value (Table I), for the front wheels the value is much lower. This phenomenon is because the peak brake torque for the front wheels exceeds the motors' limits (Fig. 12.c). Consequently, the controller activates the FB to supply the brake torque gap (Fig. 12.d). The slow EHB dynamics deteriorate the wheel slip tracking performance on the front wheels causing efficiency losses.

TABLE VI
RB AND FB ABS PERFORMANCE BENCHMARKING ON TRANSIENT SURFACE

Mode	Mean a_{Vx} on high-μ [m/s^2]	Mean a_{Vx} on low-μ [m/s^2]	$s_{braking}$ [m]	ABS_{IP} on high-μ	ABS_{IP} on low-μ
RB	9.5995	2.4844	68.1970	1.0423	1.1963
FB	8.5475	1.9648	71.8885	0.9280	0.9461

The road estimator successfully detects transient road conditions (Fig. 12.e). At the beginning, the peak deceleration is around 10 m/s^2, which refers to high-μ surface (Table I). After 4 seconds, the vehicle drives on a low-μ road, the control method resets μ* and measures peak a_{Vx} again. As the road surface has changed, the new value of μ* is recognized. Thereafter, the controller reduces the braking torques (Fig. 12.c, 12.d) to maintain the wheel slip rates close to their optimal values for a low-μ road surface (Table I).

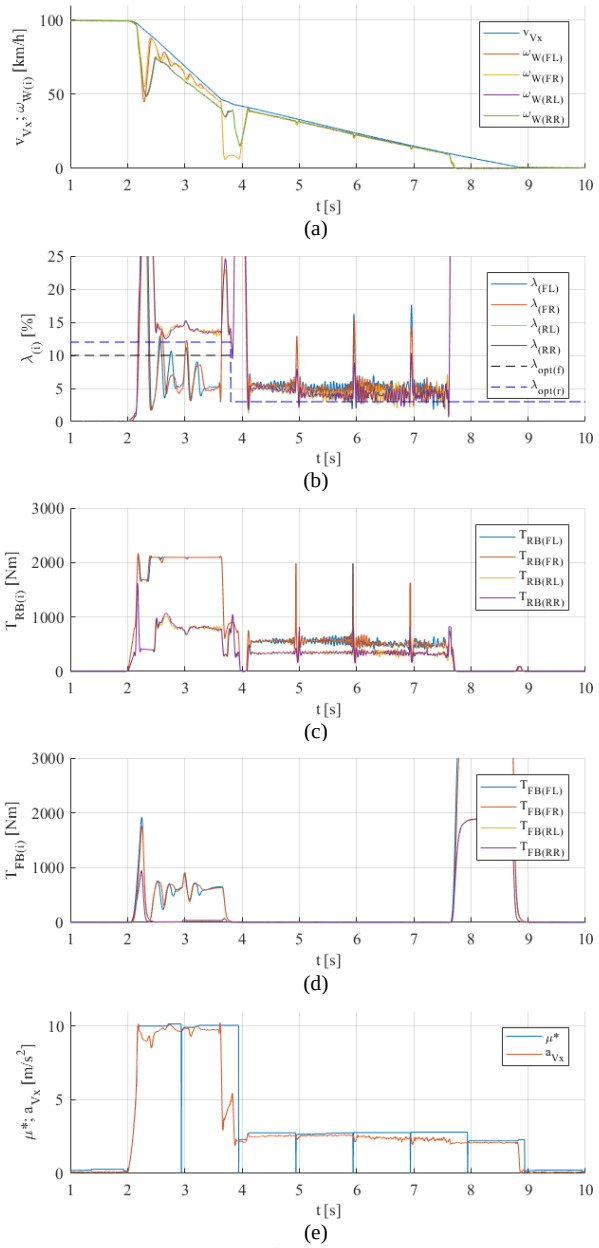

Fig. 12. Experimental results from braking on a transient road surface condition (from high-μ (μ≈1) to low-μ (μ≈0.25)) for regenerative braking: (a) vehicle and wheels speeds (b) wheels longitudinal slips; (c) RB torques; (d) FB torques; (e) road detection with vehicle body deceleration.

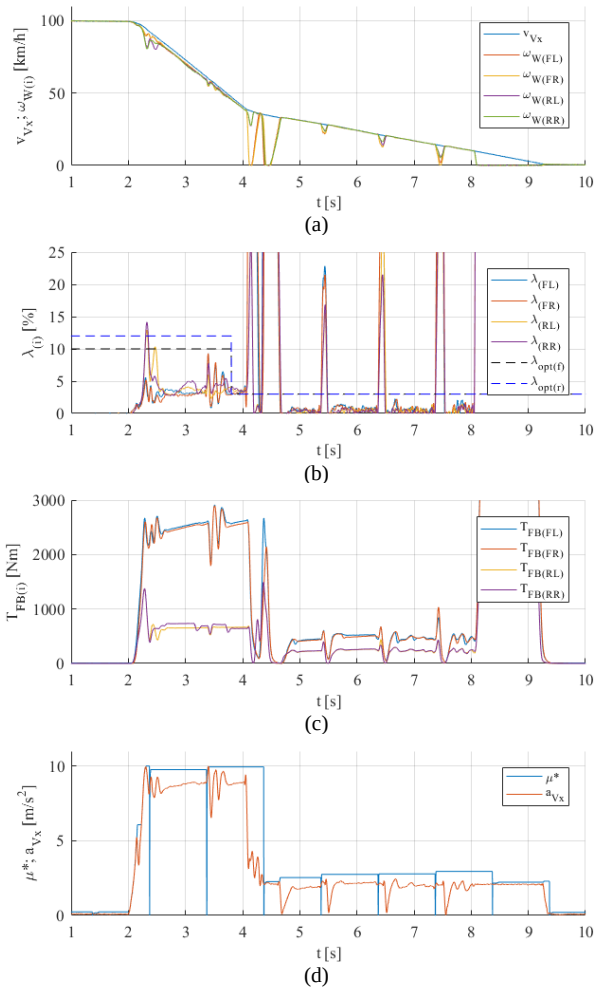

Fig. 13. Experimental results from braking on a transient road surface condition (from high-μ (μ≈1) to low-μ (μ≈0.25)) for friction braking: (a) vehicle and wheels speeds (b) wheels longitudinal slips; (c) FB torques; (d) road detection with vehicle body deceleration.

2) Friction braking

Friction braking performance results are presented in Fig. 13. The difference in optimal slip control is easily noticeable (Fig. 13.b): the EHB does not reach λ_{opt} for high-μ surface and nor keep its value on significantly lower percentage. The road estimation (Fig. 13.d) worked similar to the RB experiment. However, this time the vehicle deceleration rate is much lower.

3) Regenerative and friction braking performance comparison

A comparison of the main ABS performance indexes in the case of transient road surface conditions for RB and FB experiments is reported in Table VI. The mean vehicle decelerations in the regenerative mode are higher in comparison to the FB for both the high-μ and low-μ phases. As a result, the controller requires around 3 m shorter distance with electric motors to bring the vehicle to a full stop. Furthermore, the ABS index of performance is higher for the RB as compared to the FB for all changing road conditions tested in this experiment.

Remark 4: the wheel slip oscillations at low speeds (Fig. 10.b – 13.b) are the common problem, if the "Magic Formula" is parameterized by the experimentally obtained characteristics. Overall tire-road adhesion is a complex challenge, because its behavior is influenced by multiple parameters: speed, mass displacement, environmental conditions, tire characteristics (i.e. new, worn), etc. However, tire modeling is out of the scope of presented work.

V. Conclusion

In this paper, the development and experimental verification of an open loop fuzzy-logic-based control method with road surface recognition feature for a novel decoupled electro-hydraulic ABS is presented. The HIL set-up consists of an EHB connected to a host PC through a dSPACE® electronic platform. The PC runs the IPG CarMaker® software containing an experimentally validated model of e-SUV. The HIL system is capable of reproducing real pressure dynamics in the brake circuit, whereas the vehicle dynamics are rendered by the e-SUV numerical model.

The EHB's slower comparing to the on-board electric motor dynamics take a tool on the controller tracking performance: in case of pure conventional FB utilization, the controller exhibits significant lower performance. Despite, identical FLC design for both FB and RB actuators, fast dynamics of the motor allow for more accurate tracking of the optimal wheel slip. As a result, the mean vehicle decelerations in full RB mode are higher in comparison with the decoupled EHB system for both high-μ and low-μ surfaces. Furthermore, the ABS index of performance also proves that the controller in case of full braking regeneration performs better than in the case of pure FB utilization. In the future, the FLC-based ABS control method will be tested on an experimental e-SUV.

Acknowledgment

This project has received funding from the European Union's Horizon 2020 research and innovation program under grant agreement No. 675999. The authors would also like to express their sincere gratitude to Dr. Dzmitry Savitski from Arrival Germany GmbH, (Pforzheim, Germany) for consultation on hardware-in-the-loop test rig operation.

References

[1] W. Post, "Car braking systems," in K. Reif (Ed.), *Brakes, Brake Control and Driver Assistance Systems: Function, Regulation and Components*, Wiesbaden, Germany: Springer Vieweg, 2014, pp. 28–39. DOI: 10.1007/978-3-658-03978-3

[2] E. Regolin, G. P. Incremona, and A. Ferrara, "Longitudinal vehicle dynamics control via sliding modes generation," in A. Ferrara (Ed.), *Sliding Mode Control of Vehicle Dynamics*, IET Digital Library, 2017, pp. 33–76. DOI: 10.1049/PBTR005E

[3] D. Savitski, D. Shleinin, V. Ivanov, and K. Augsburg, "Robust continuous wheel slip control with reference adaptation: Application to the brake system with decoupled architecture," *IEEE Trans. on Indust. Inform.*, vol. 14, no. 9, pp. 4212–4223, April 2018. DOI: 10.1109/TII.2018.2817588

[4] F. Pretagostini, B. Shyrokau, and G. Berardo "Anti-lock braking control design using a Nonlinear Model Predictive approach and wheel information," in *IEEE Intern. Conf. on Mechat. (ICM)*, Ilmenau, Germany, 2019, pp. 525–530. DOI: 10.1109/ICMECH.2019.8722841

[5] D. Tavernini, F. Vacca, M. Metzler, D. Savitski, V. Ivanov, P. Gruber, A. E. H. Karci, M. Dhaens, and A. Sorniotti, "An explicit nonlinear model predictive ABS controller for electro-hydraulic braking systems," *IEEE Trans. on Indust. Elect.*, Early Access, May 2019. DOI: 10.1109/TIE.2019.2916387

[6] M. Tanelli, A. Astolfi, and S. M. Savaresi, "Robust nonlinear proportional-integral control for active braking control systems," *in 45th IEEE Conf. on Decision and Control*, San Diego, USA, 2006. DOI: 10.1109/CDC.2006.377194

[7] S. Ç. Başlamişli, İ. E. Köse, and G. Anlaş, "Robust control of anti-lock brake system," *Intern. J. of Veh. Mech. and Mobility: Veh. Syst. Dynamics*, vol. 45, no. 3, pp. 217–232, Sept. 2007. DOI: 10.1080/00423110600882498

[8] C.-M. Lin and C.-F. Hsu, "Self-Learning fuzzy sliding-mode control for antilock braking systems," *IEEE Trans. on Cont. Syst. Tech.*, vol. 11, no. 2, pp. 273–278, Mar. 2003. DOI: 10.1109/TCST.2003.809246

[9] C.-M. Lin and H.-Y. Li, "Intelligent hybrid control system design for antilock braking systems using self-organizing function-link fuzzy cerebellar model articulation controller," *IEEE Trans. on Fuzzy Syst.*, vol. 21, no. 6, pp. 1044–1055, Jan. 2013. DOI: 10.1109/TFUZZ.2013.2241769

[10] J. Guo, X. Jian, and G. Lin, "Performance evaluation of an anti-lock braking system for electric vehicle with fuzzy sliding mode controller," *Energies*, vol. 7, no. 10, pp. 6459–6476, Aug. 2014. DOI: 10.3390/EN7106459

[11] K. Jalali, T. Uchida, J. McPhee, and S. Lambert, "Development of a fuzzy slip control system for electric vehicles with in-wheel motors," *SAE Int. J. of Alternative Powertrains*, vol. 1, no. 1, pp. 46–64, June 2012. DOI: 10.4271/2012-01-0248

[12] H.-Z. Li, L. Li, L. He, M.-X. Kang, J. Song, L.-Y. Yu, and C. Wu, "PID plus fuzzy logic method for torque control in traction control system," *Int. J. Automotive Technology*, vol. 13, no. 3, pp. 441–450, Apr. 2012. DOI: 10.1007/S12239-012-0041-4

[13] S. L. Peric, D. S. Antic, M. B. Milovanovic, D. B. Mitic, M. T. Milojkovic, and S. S. Nikolic, "Quasi-sliding mode control with orthogonal endocrine neural network-based estimator applied in anti-lock braking system," *IEEE/ASME Trans. on Mechatronics*, vol. 21, no. 2, pp. 754–764, Apr. 2016. DOI: 10.1109/TMECH.2015.2492682

[14] H. Chen, J. Yang, Z. Du, and W. Wang, "Adhesion control method based on fuzzy logic control for four-wheel-driven electric vehicle," *SAE Int. J. Passeng. Cars – Mech. Syst.*, vol. 3, no. 1, pp. 217–225, Apr. 2010. DOI: 10.4271/2010-01-0109

[15] P. Khatun, C. M. Bingham, N. Schofield, and P. H. Mellor, "Application of fuzzy control algorithms for electric vehicle antilock braking/traction control systems," *IEEE Trans. on Veh. Tech.*, vol. 52, no. 5, pp. 1356–1364, Sep. 2013. DOI: 10.1109/TVT.2003.815922

[16] X. Peng, M. Jia, L. He, X. Yu, and Y. Lv, "Fuzzy sliding mode control based on longitudinal force estimation for electro-mechanical braking systems using BLDC motor," *CES Trans. on Elect. Machines and Syst.*, vol. 2, no. 1, pp. 142–151, Mar. 2018. DOI: 10.23919/TEMS.2018.8326461

[17] J. A. Cabrera, A. Ortiz, J. J. Castillo, and A. Simón, "A fuzzy logic control for antilock braking system integrated in the IMMa tire test bench," *IEEE Trans. on Veh. Tech.*, vol. 54, no. 6, pp. 1937–1949, Nov. 2005. DOI: 10.1109/TVT.2005.853479

[18] J. J. Castillo, J. A. Cabrera, A. J. Guerra, and A. Simón, "A novel electrohydraulic brake system with tire-road friction estimation and continuous brake pressure control," *IEEE Trans. on Indust. Electr.*, vol. 63, no. 3, pp. 1863–1875, Mar. 2016. DOI: 10.1109/TIE.2015.2494041
[19] S.-J. Huang and W.-C. Lin, „Adaptive fuzzy controller With sliding surface for vehicle suspension control," *IEEE Trans. on Fuzzy Syst.*, vol. 11, no. 4, pp. 550–559, Aug. 2003. DOI: 10.1109/TFUZZ.2003.814845
[20] O. Cerman and P. Hušek, „Adaptive fuzzy sliding mode control for electro-hydraulic servo mechanism," *Expert Syst. with Applic.*, vol. 39, no. 1, pp. 10269–10277, Sep. 2012. DOI: 10.1016/j.eswa.2012.02.172
[21] H. Du and N. Zhang, „Fuzzy control for nonlinear uncertain electrohydraulic active suspensions with input constraint," *IEEE Trans. on Fuzzy Syst.*, vol. 17, no. 2, pp. 550–559, April 2009. DOI: 10.1109/TFUZZ.2008.2011814
[22] X. Wu, C. Ma, M. Xu, Q. Zhao, and Z. Cai, "Single-parameter skidding detection and control specified for electric vehicle," *J. of the Franklin Inst.*, vol. 352, no. 2, pp. 724–743, 2015. DOI: 10.1016/j.jfranklin.2014.07.007
[23] V. Schreiber, V. Ivanov, K. Augsburg, M. Noack, B. Shyrokau, C. Sandu, and P.S. Els, "Shared and distributed X-in-the-loop tests for automotive systems: Feasibility study," *IEEE Access*, vol. 6, pp. 4017–4026, 2018. DOI: 10.1109/ACCESS.2017.2789020
[24] D. Bullock, B. Johnson, R. B. Wells, M. Kyte, and Z. Li, "Hardware-in-the-loop simulation," *Transp. Res. Part C: Emerging Tech.*, vol. 12, no. 1, pp. 73–89, 2004. DOI: 10.1016/j.trc.2002.10.002
[25] V. Ivanov, "A review of fuzzy methods in automotive engineering applications," *Eur. Transp. Res. Rev.*, vol. 7, no. 29, pp. 1–10, Sep. 2015. DOI: 10.1007/S12544-015-0179-Z
[26] C.-Y. Chen, L.-Q. Liu, C.-C. Cheng, and G. T.-C. Chiu, "Fuzzy controller design for synchronous motion in a dual-cylinder electro-hydraulic system," *Cont. Eng. Practice*, vol. 16, no. 6, pp. 658–673, June 2008. DOI: 10.1016/j.conengprac.2007.08.005
[27] S. Y. Lee and H. S. Cho, "A fuzzy controller for an electro-hydraulic fin actuator using phase plane method," *Cont. Eng. Practice*, vol. 11, no. 6, pp. 697–708, June 2003. DOI: 10.1016/S0967-0661(02)00179-X
[28] M. E.-S. M. Essa, M. A. S. Aboelela, M. A. M. Hassan, and S. M. Abdrabbo, "Control of hardware implementation of hydraulic servo application based on adaptive neuro fuzzy inference system," *in 14th Intern. Comp. Eng. Conf. (ICENCO)*, Cairo, Egypt, 2018. DOI: 10.1109/ICENCO.2018.8636112
[29] W. M. Bessa. M. S. Dutra, and E. Kreuzer, "Sliding mode control with adaptive fuzzy dead-zone compensation of an electro-hydraulic servo-system," *J. of Intel. and Rob. Syst.*, vol. 58, no. 1, pp. 3–16, April 2010, DOI: 10.1007/S10846-009-9342-X
[30] A. Aksjonov, V. Vodovozov, K. Augsburg, and E. Petlenkov, "Design of regenerative anti-lock braking system controller for 4-in-wheel-motor drive electric vehicle with road surface estimation," *Int. J. Automotive Technology*, vol. 19, no. 4, pp. 727–742, Aug. 2018. DOI: 10.1007/S12239-018-0070-8
[31] D. Savitski, V. Ivanov, K. Augsburg , B. Shyrokau, R. Wragge-Morley, T. Pütz, and P. Barber, "The new paradigm of an anti-lock braking system for a full electric vehicle: experimental investigation and benchmarking," *Proc. Institution. Mech. Eng. Part D, J. Autom. Eng.*, vol. 230, no. 10, pp. 1364–1377, 2016. DOI: 10.1177/0954407015608548
[32] K. M. Passino and S. Yurkovich, *Fuzzy Control*, Menlo Park, California, USA: Addison-Wesley Longman, Inc., 1998, pp. 1–22, 23–118.
[33] V. Ricciardi, D. Savitski, K. Augsburg, and V. Ivanov, "Estimation of brake friction coefficient for blending function of base braking control," *SAE Int. J. Passeng. Cars – Mech. Syst.*, vol. 10, no. 3, pp. 774–785, 2017. DOI: 10.4271/2017-01-2520
[34] U. Kiencke and L. Nielsen, *Automotive Control Systems: For Engine, Driveline, and Vehicle*, 2nd ed., Berlin, Germany: Springer-Verlag Berlin Heidelberg, 2005, pp. 301–350, 351–408, 409–424. DOI: 10.1007/b137654
[35] A. Aksjonov, P. Nedoma, V. Vodovozov, E. Petlenkov, and M. Herrmann, "A method of driver distraction evaluation using fuzzy logic Phone usage as a driver's secondary activity: Case study," in *26th Intern. Conf. on Inform., Commun. and Autom. Techn. (ICAT)*, Sarajevo, Bosnia & Herzegovina, 2017, pp. 23–28. DOI: 10.1109/ICAT.2017.8171599
[36] O. Castillo, *Type-2 Fuzzy Logic in Intelligent Control Applications*, Berlin: Springer-Verlag Berlin Heidelberg, 2012, pp. 49–61.
[37] J. J. Castillo, J. A. Cabrera, A. J. Guerra, and A. Simón, "A novel electrohydraulic brake system with tire-road friction estimation and continuous brake pressure control," *IEEE Trans. on Indust. Elect.*, vol. 63, no. 3 pp. 1863–1875, March 2016. DOI: 10.1109/TIE.2015.2494041

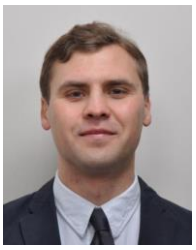

Andrei Aksjonov (M'-) received his BSc, MSc and PhD degrees in electrical engineering with automation specialization from Tallinn University of Technology, Estonia. He is a Marie Skłodowska-Curie research fellow hosted by Škoda Auto, Czech Republic. His research interests include computational intelligence, vehicle dynamics control, vehicle safety, human-machine interface.

Vincenzo Ricciardi (M'-) received his BSc and MSc in Mechanical Engineering from the University of Salerno, Italy in 2012 and 2014 respectively. He started his professional career in collaboration with Magneti Marelli Powertrain (Bologna, Italy). He is currently a Marie Skłodowska-Curie research fellow at the Technische Universität Ilmenau, Germany. His research interests include advanced vehicle control, state estimation, and analysis of brake-related emissions.

Klaus Augsburg received the Dr.-Ing. Degree from Technische Universität Dresden, Germany, in 1985. From 1984 to 1993, he was with industry on leading engineer positions and then from 1993 to 1999 as a Senior Assistant with Technische Universität Dresden, Germany. In 1999, he was a Full Professor and the Chair of Automotive Engineering Group, Technische Universität Ilmenau, Germany. In 2011, he founded Thuringian Centre of Innovation in Mobility. He has authored over 100 research papers, guest lectures, and patents. He is a member of the Association of German Engineers, the Chairman of Workgroup Automotive Engineering VDI Thüringen, and the CEO of Steinbeis-Transferzentrum Fahrzeugtechnik.

Valery Vodovozov (M'-) received the Candidate of Science degree from Saint Petersburg Electrotechnical University, Russia. He also served in the same institution as an Associate Professor and a Senior Researcher in electrical engineering. He is currently a Senior Lecturer with Tallinn University of Technology, Estonia. His research interests include power electronics and electrical drives areas. He is a member of the International Institute of Informatics and Systemics and the Global Research Alliance of Texas Institute of Science.

Eduard Petlenkov received his BSc, MSc and PhD degrees in computer and systems engineering from Tallinn University of Technology, Estonia. He is a Professor in the Department of Computer Systems at Tallinn University of Technology. His main research interests include computational intelligence, nonlinear control, and system analysis.